

Electron-injecting properties of Rb₂CO₃-doped Alq₃ thin films in organic light-emitting diodes

Jin Woo Park, Jong Tae Lim, Jong Sik Oh, Sung Hee Kim, Phuong Pham Viet et al.

Citation: *J. Vac. Sci. Technol. A* 31, 031101 (2013); doi: 10.1116/1.4798302

View online: <http://dx.doi.org/10.1116/1.4798302>

View Table of Contents: <http://avspublications.org/resource/1/JVTAD6/v31/i3>

Published by the AVS: Science & Technology of Materials, Interfaces, and Processing

Additional information on J. Vac. Sci. Technol. A

Journal Homepage: <http://avspublications.org/jvsta>

Journal Information: http://avspublications.org/jvsta/about/about_the_journal

Top downloads: http://avspublications.org/jvsta/top_20_most_downloaded

Information for Authors: http://avspublications.org/jvsta/authors/information_for_contributors

ADVERTISEMENT



AMERICAN
ELEMENTS

Now Invent.TM

The World's Manufacturer
of Engineered &
Advanced Materials

www.americanelements.com

Electron-injecting properties of Rb_2CO_3 -doped Alq_3 thin films in organic light-emitting diodes

Jin Woo Park, Jong Tae Lim, Jong Sik Oh, and Sung Hee Kim

School of Advanced Materials Science and Engineering, Sungkyunkwan University, Suwon 440-746, South Korea

Phuong Pham Viet

SKKU Advanced Institute of Nano-Technology (SAINT), Sungkyunkwan University, Suwon 440-746, South Korea

Myung S. Jhon

Department of Chemical Engineering and Data Storage Systems Center, Carnegie Mellon University, Pittsburgh, Pennsylvania 15213

Geun Young Yeoma^a

School of Advanced Materials Science and Engineering, Sungkyunkwan University, Suwon 440-746, South Korea and SKKU Advanced Institute of Nano-Technology (SAINT), Sungkyunkwan University, Suwon 440-746, South Korea

(Received 12 October 2012; accepted 11 March 2013; published 3 April 2013)

Rubidium carbonate (Rb_2CO_3)-doped tris(8-quinolinolato)aluminum (III) (Alq_3) thin films have been investigated as electron-injecting materials for organic light-emitting diodes (OLEDs). Electron-only devices consisting of glass/tin-doped indium oxide (ITO)/ Rb_2CO_3 -doped Alq_3 (10 nm)/aluminum (Al) showed an electron-ohmic contact property between the electrode and the organic layer at the doping concentration of 10% and higher. The electron-injecting ability of these contacts was largely enhanced by the *n*-doping effect of Rb_2CO_3 into the Alq_3 layer. The ultraviolet photoemission spectra revealed that when the doping concentration was increased, the *n*-doping effect reduced the carrier-injecting barrier height by lowering the work function at the Rb_2CO_3 -doped Alq_3 interfaces. Also, the x-ray photoemission spectra showed that as the doping concentration was increased at the interfaces, Alq_3 molecules decomposed in a chemical reaction with Rb_2CO_3 . The OLED device, having the glass/ITO/molybdenum oxide (MoO_x , 25%)-doped *N,N'*-diphenyl-*N,N'*-bis(1-naphthyl)-1,1'-biphenyl-4,4'-diamine (NPB, 5 nm)/NPB (63 nm)/ Alq_3 (32 nm)/ Rb_2CO_3 -doped Alq_3 (10%, 10 nm)/Al (100 nm) structure, showed the best performance at the optimal doping concentration of Rb_2CO_3 -doped Alq_3 , both the maximum luminance of 114 400 cd/m² at the bias voltage of 9.8 V and the power efficiency of 2.7 lm/W at the luminance of 1000 cd/m² were obtained. © 2013 American Vacuum Society. [http://dx.doi.org/10.1116/1.4798302]

I. INTRODUCTION

Recently, organic semiconductors such as organic light-emitting diodes (OLEDs), organic solar cells, organic thin film transistors, and organic sensors have attracted much attention due to their potential in optoelectronic applications.^{1–4} Among these devices, OLEDs are actively investigated for next generation applications such as lighting, flexible displays, transparent displays, etc.⁵ One of the critical issues in fabricating high-performance OLEDs is the improvement of the carrier injection efficiency at the electrode/organic interfaces. This carrier-injecting efficiency greatly depends upon the number of carriers and the carrier-injecting barrier height (Φ_B^e) at the interfaces between the metal and organic layers.⁶ Therefore, developing an efficient carrier-injecting layer between the metal and the organic layers is one of the key elements in improving the light-emitting efficiency of OLEDs.⁷

Doping techniques for carrier-injecting layers have been extensively investigated in the development of an efficient carrier-injecting layer in *p-i-n* OLEDs, in which an intrinsic

emission layer is embedded between the *p*-type and the *n*-type doped layer.^{8–13} Recently, metal oxide-based *p*-doping materials, such as molybdenum oxide (MoO_3), rhenium oxide (ReO_3), vanadium oxide (V_2O_5), and tungsten oxides (WO_3), have been developed to form the hole-injecting layer (HIL).^{14–18} Meanwhile, alkali-metal carbonates, such as rubidium carbonate (Rb_2CO_3), cesium carbonate (Cs_2CO_3), and lithium carbonate (Li_2CO_3), have been investigated as *n*-type dopants to form the electron-injecting layer (EIL).^{19–21} Chen *et al.* reported that the *n*-doping effect of Rb_2CO_3 in a 4,7-diphenyl-1,10-phenanthroline (Bphen)/ Rb_2CO_3 /Al system can improve the electron conductivity between the electron-transporting layer (ETL) and the electrode in OLEDs through an energy level study and a theoretical calculation of the gap states formed at this interface.¹⁹ These doping materials lead to the formation of an ohmic contact between the electrode and the carrier-injecting layer. Also, *p-i-n* OLEDs with a carrier-injecting layer has a low driving voltage with high carrier conductivity, and therefore, high efficiency.^{11,22}

Even though the previous study¹⁹ demonstrated that the *n*-doping effect of Rb_2CO_3 on Bphen can improve the

^aElectronic mail: gyeom@skku.edu

contact property between the electrode and the carrier-injecting layer, it is difficult to apply Rb₂CO₃ as the ETL material for OLEDs, especially in actual field operation, due to its low glass transition temperature (T_g) and low reliability in high temperature operations. Among the various materials, Alq₃ is the most commonly investigated ETL material; therefore, it is important to understand the *n*-doping effect of Rb₂CO₃ on Alq₃, which is similar to the *n*-doping effect of Rb₂CO₃ on Bphen. Therefore, in this study, the *n*-doping effect of Rb₂CO₃ on Alq₃ has been investigated. Especially, the electron-injecting properties and electronic structure of Rb₂CO₃-doped Alq₃ thin films as EILs were investigated, and these thin films were applied as electron-ohmic contacts in OLEDs. The *n*-doping effect of the Rb₂CO₃-doped Alq₃ layer as an EIL at different doping concentrations and different thicknesses was investigated by reviewing the electron-ohmic contact property of electron-only devices. Also, the interfacial electronic structure that originated from the *n*-doping effect, which can be used to understand both Φ_B^c and the interface mechanism, was investigated by using x-ray photoemission spectroscopy (XPS) and ultraviolet photoemission spectroscopy (UPS). Finally, the correlation between the physical properties of the Rb₂CO₃-doped Alq₃ thin film and the device performance of the carrier-ohmic OLED was discussed.

II. EXPERIMENT METHODS

OLEDs were constructed with glass/tin-doped indium oxide (ITO, about $10\ \Omega/\square$)/molybdenum oxide (MoO_x, 25%)-doped *N,N'*-diphenyl-*N,N'*-bis(1-naphthyl)-1,1'-biphenyl-4,4'-diamine (NPB, 5 nm)/NPB (63 nm)/tris(8-quinolinolato) aluminum (III) (Alq₃, 42-y nm)/rubidium carbonate (Rb₂CO₃, x%)-doped Alq₃ (y nm)/aluminum (Al, 100 nm). In the Rb₂CO₃-doped Alq₃ thin film, the Rb₂CO₃ doping concentration was varied as 0, 2.5, 10, and 50% and the film thickness was varied as 10, 20, 30, and 40 nm at the optimal doping concentration of Rb₂CO₃. MoO_x-doped NPB was used for the HIL,²³ NPB for the hole-transporting layer, Alq₃ for the emissive layer (EML) and the ETL, Alq₃ doped with Rb₂CO₃ for the EIL, and Al for the cathode layer. A multilayer of MoO_x-doped NPB/NPB/Alq₃/Rb₂CO₃-doped Alq₃/Al was formed by *in-situ* deposition through sequential thermal evaporation on a glass/ITO substrate. The doped carrier-injecting layers such as Rb₂CO₃-doped Alq₃ and MoO_x-doped NPB were formed by coevaporation of host and dopant materials. The emissive active areas of all devices were $2 \times 2\text{ mm}^2$. The electron-only devices were fabricated separately from the structure of glass/ITO/Rb₂CO₃-doped Alq₃ (x%, y nm)/Al (100 nm). The doping concentration (x %) of Rb₂CO₃ was varied from 0 to 50%, and the thickness of Rb₂CO₃-doped Alq₃ thin film was also varied from 10 to 40 nm. The same experiments were repeated more than three times due to the high air sensitivity of the alkali metals during device fabrication, but the differences of the measured data among the experiments were less than 10% in general.

The current density–voltage–luminance (J-V-L) and J-V characteristics of the fabricated devices were measured using

an electrometer (Keithley 2400 or Hewlett Packard 4145A), a silicon photodiode (Oriel 71608), and a picoammeter (Keithley 485). The electronic structures of the Rb₂CO₃-doped Alq₃ thin films were examined using XPS and UPS at the 4D beam line of the Pohang Accelerator Laboratory in Korea. The depositions and measurements were performed in an ultrahigh vacuum system, consisting of a main analysis chamber (approximately, $5 \times 10^{-10}\text{ Torr}$) and a sample preparation chamber (approximately, $5 \times 10^{-9}\text{ Torr}$). For the analysis, Rb₂CO₃-doped Alq₃ (10 nm) thin films of various doping concentrations were prepared *in-situ* by sequential thermal evaporation on a *p*-type Si wafer in an ultrahigh vacuum system, which was connected to the beam line in a vacuum. The thicknesses of the deposited thin films were obtained by timed depositions, calibrated using a quartz-crystal microbalance. In the XPS study, incident photon energy of 350 eV was used to obtain the core level spectra of Al 2p. For the UPS measurement, the ultraviolet source of He I (21.2 eV) line was used. The photoemission onset, reflecting the work function (Φ) at the surface of a sample, was measured by biasing the sample at -5.0 V . The incident photon energy was calibrated by measuring the Au 4f level of the Au surface.

III. RESULTS AND DISCUSSION

As there are no intrinsic charge carriers in organic materials, all holes and electrons have to be injected from an anode and cathode, respectively. Therefore, charge injection efficiency and interface stability control the overall device performance of an OLED. To obtain a low driving voltage and to eliminate Joule heating at the organic layer/electrode interface, it is essential to build a robust interface with no potential barrier.²⁴ In order to establish a robust ohmic contact between the organic layer and the cathode, a series of electron-only devices with the Rb₂CO₃-doped Alq₃ thin film were designed, and their electrical characteristics were investigated as functions of the Rb₂CO₃ doping concentration in Alq₃ and the thickness of the Rb₂CO₃-doped Alq₃ thin film. Essentially, an electron-only device can be defined as a device with the electron as the major carrier.

Figure 1(a) shows the J-V characteristics of the electron-only devices as a function of the Rb₂CO₃ doping concentration in the 10 nm-thick Rb₂CO₃-doped Alq₃ layer. The device structure was glass/ITO/Rb₂CO₃-doped Alq₃ (x%, 10 nm; x = 0, 2.5, 10, and 50)/Al (100 nm). A bias voltage was applied to the bottom electrode in reference to the top ground electrode. When the doping concentration is 10% or higher, the electron-only devices exhibit a perfectly linear line, with the characteristics of a true ohmic contact at both the top and bottom interfaces.²⁵ However, when the doping concentration of Rb₂CO₃ is either below 10% (ITO/Rb₂CO₃-doped Alq₃/Al) or when the Alq₃ layer is pristine (ITO/Alq₃/Al), the current density–voltage curves of the devices are nonlinear, indicating nonohmic and highly resistive contact characteristics. Also, when the doping concentration is higher than 10%, the J-V characteristics degrade, showing higher resistivity in regards to the contact at higher doping

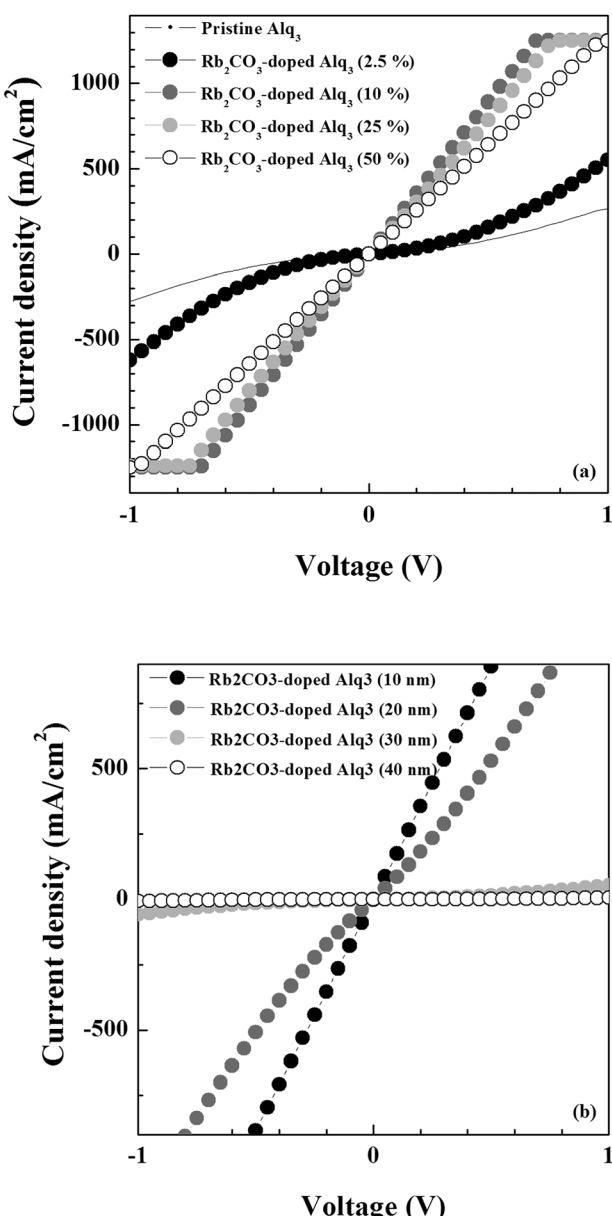


FIG. 1. Current density–voltage characteristics of the electron-only devices both as a function of the Rb₂CO₃ doping concentration in the 10 nm-thick Rb₂CO₃-doped Alq₃ layer (a) and as a function of the thickness of the Rb₂CO₃-doped Alq₃ thin film at the doping concentration of 10% (b). The device structure was glass/ITO/Rb₂CO₃-doped Alq₃ (x%; y nm; x = 0, 2.5, 10, and 50; y = 10, 20, 30, and 40)/Al (100 nm). The bias was applied to the bottom electrode in reference to the top grounding electrode.

concentrations. This observation reveals that electron conductivity is strongly dependent on the doping concentration of Rb₂CO₃. In addition, the near symmetric J-V characteristics obtained in our experiment even with different electrodes (ITO and Al) might be related to the tunneling current from the ITO side (Φ is \sim 4.7 eV) to the Rb₂CO₃ doped Alq₃ layer during application of negative voltage to the ITO electrode while the Al electrode is grounded. On the other hand, when a positive voltage is applied to the ITO electrode while the Al electrode is grounded, electrons are believed to be injected when they jump the energy difference between the lowest unoccupied molecular orbital (LUMO) levels of the Rb₂CO₃-doped Alq₃ and Al (Φ is \sim 4.3 eV).

Figure 1(b) exhibits the J-V characteristics of the electron-only devices measured as a function of the thickness of the Rb₂CO₃-doped Alq₃ thin film at the doping concentration of 10%. The device structure was glass/ITO/Rb₂CO₃-doped Alq₃ (10%, y nm; y = 10, 20, 30, and 40)/Al (100 nm). As shown in the figure, the J-V characteristics of the electron-only devices demonstrated the best performance when the Rb₂CO₃-doped Alq₃ thin film was the thinnest (10 nm). When the Rb₂CO₃-doped Alq₃ thin film was thicker than 30 nm, the J-V characteristics became very resistive and even showed slightly nonlinear characteristics. The increased resistive J-V characteristics with the increase of the Rb₂CO₃-doped Alq₃ thin film thickness are believed to be related to the increased resistance of the film. Therefore, the electron-injecting layer demonstrated the best performance when the electron density at the interface was increased without an increase in the series resistance of the device at Rb₂CO₃-doped Alq₃ thin film thickness of 10 nm and doping concentration of 10%. In fact, the increase of voltage with increasing thickness of the Rb₂CO₃-doped Alq₃ thin film at a given current density also tells us that the electrical conduction of the electron-only device with the 10% Rb₂CO₃-doped Alq₃ thin film is bulk-limited conduction not interface-limited conduction due to the efficient electron injection at the interface for the 10% Rb₂CO₃-doped Alq₃ thin film. For bulk-limited conduction, ohmic conduction, trap-filled limited conduction, and space charge limited conduction will follow the relationships of $V \propto$ thickness, $V \propto$ thickness², and $V \propto$ thickness^{3/2}, respectively.²⁶ However, due to the lack of data, the exact bulk-limited conduction mechanism could not be identified in this experiment.

In order to further understand the J-V characteristics of the electron-only devices investigated in Fig. 1(a) as a function of Rb₂CO₃ doping concentration in the Rb₂CO₃-doped Alq₃ thin film, the interface characteristics between the Rb₂CO₃-doped Alq₃ thin film and electrodes were investigated for the electron injection mechanism at the interface. Figure 2(a) shows the electron density curves of the Al 2p core level XPS for both pristine Alq₃ and Rb₂CO₃-doped Alq₃ thin films with various Rb₂CO₃ doping concentrations on *p*-type Si wafers. The film thickness was maintained at 10 nm. The peak at 74 eV in the figure is from the Al 2p XPS spectrum of the nondoped Alq₃.²⁷ As the concentration of the Rb₂CO₃ in the film increased, a new peak related to a species decomposed by chemical reactions is observed from 10% of Rb₂CO₃ at the lower binding energy of 73.3 eV, and this peak increases with increasing concentration of the Rb₂CO₃ dopant in the film, indicating increases in chemical reactions. This peak also gradually broadens. Therefore, as shown in the Al 2p XPS spectra, the Alq₃ molecule itself begins to slowly decompose, starting at 10% Rb₂CO₃ doping concentration, and becomes seriously decomposed at 50% Rb₂CO₃ doping concentration. Similar phenomena were also observed for the electronic features of the Al-on-Alq₃ interfaces investigated by Mason *et al.*²⁸

The slightly decomposed species of Alq₃ will function as the electrical conductor with the metallic structures. When the doping concentration of Rb₂CO₃ is less than 10%, Alq₃

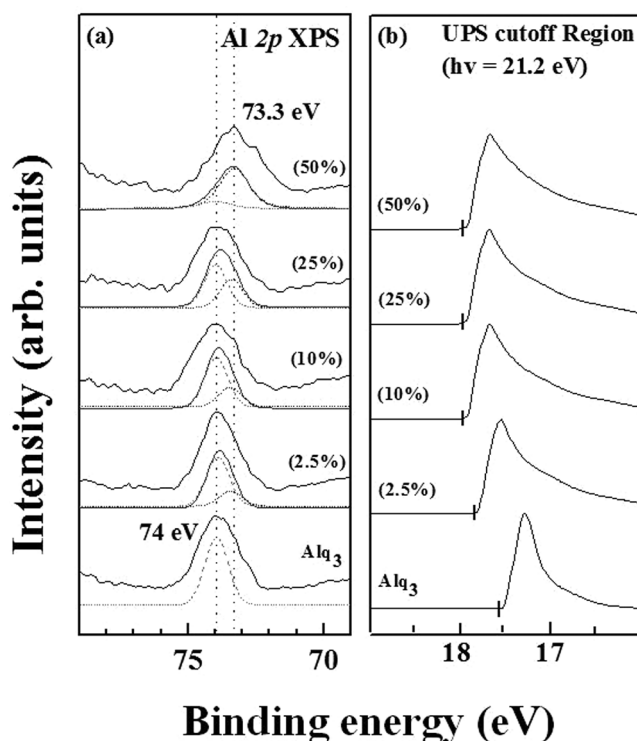


Fig. 2. Al 2p core level XPS spectra of the Rb₂CO₃-doped Alq₃ thin film (a) and the onset of the work function in the UPS spectra (b) as a function of Rb₂CO₃ doping concentration. The bottom curves in (a) are deconvoluted peaks at 74 and 73.3 eV for the Al 2p core level XPS peak.

appears to be not decomposed, except for the formation of a stable Alq₃⁻³ radical anion through the acceptance of electrons from the Rb metal in Rb₂CO₃ caused by the nonstoichiometric Rb₂CO₃ deposition.²⁸ However, when the concentration of Rb₂CO₃ is equal to or higher than 10%, Alq₃ appears to be decomposed by the strong reaction between Rb₂CO₃ (as an electron donor) and Alq₃ (as an

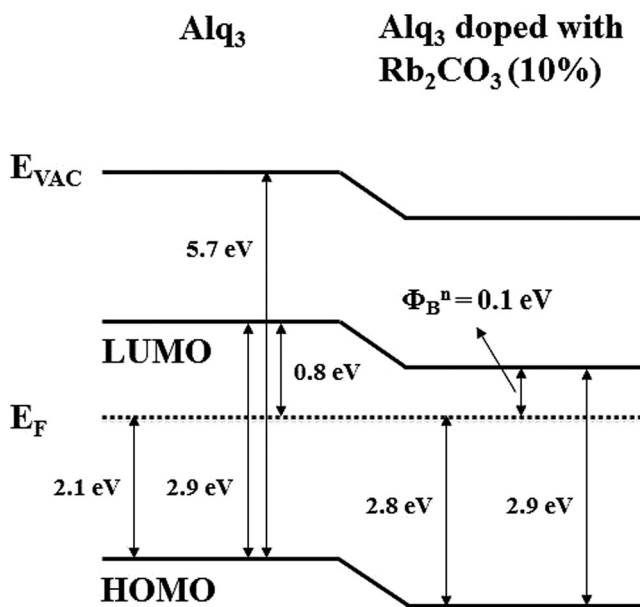


Fig. 3. Proposed energy band diagrams of the pristine Alq₃ and Rb₂CO₃-doped Alq₃ thin films. The doping concentration of Rb₂CO₃ was 10%.

electron acceptor), similar to the Cs₂CO₃-doped Alq₃ system.²⁰ Furthermore, considering that the Al atom in the saturated Alq₃ molecule has six-coordinate numbers by three chelate ligands, the structural destruction of Alq₃ exposes the Al atom in the Alq₃ molecule. These phenomena lead to a marked increase in the free carrier concentration in the doped layer and are related to the formation of the ohmic contact observed in electron-only devices with Rb₂CO₃ doping concentrations of 10% and above. However, the severe decomposition of the Alq₃ thin film increased the defects in the film; therefore, it decreased the free carrier concentration in the film and worked as a resistor, especially when the doping concentration was higher than 10%.

Figure 2(b) shows the onset of the Φ in the pristine Alq₃ film and in Rb₂CO₃-doped Alq₃ thin film as a function of the Rb₂CO₃ doping concentration in the UPS spectra. Compared to Φ in the pristine Alq₃, at the initial doping concentration of 2.5%, Φ was significantly reduced to 0.4 eV compared to that of pristine Alq₃. This abrupt reduction of Φ is related to

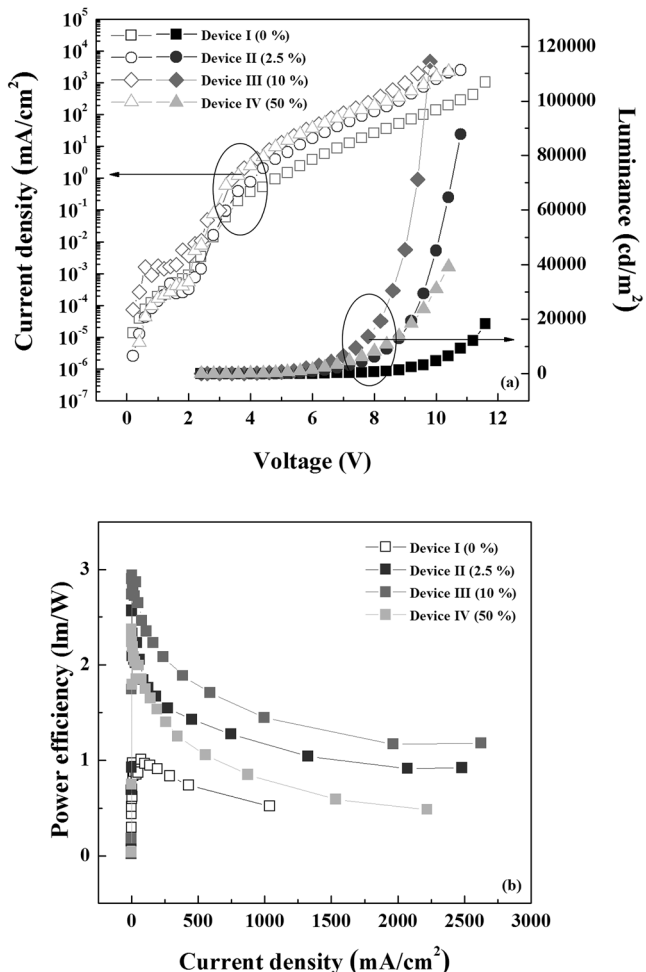


Fig. 4. (a) Current density–voltage–luminance characteristics in OLEDs with all carrier-ohmic contacts measured as a function of the Rb₂CO₃ doping concentration in the Rb₂CO₃-doped Alq₃ thin film. The device structure was glass/ITO/MoO_x-doped NPB (25%, 5 nm)/NPB (63 nm)/Alq₃ (32 nm)/Rb₂CO₃-doped Alq₃ (x%, 10 nm)/Al (100 nm). The doping concentrations of Rb₂CO₃ in devices I, II, III, and IV were 0, 2.5, 10, and 50%, respectively. (b) Power efficiency measured as a function of a current density.

the charge exchanges and a strong dipole field at the interface between Alq₃ and Rb₂CO₃.²⁰ The Φ is further decreased with the increase of Rb₂CO₃ doping concentration to 10%; however, the further increase of the doping concentration from 10 to 50% does not change Φ significantly, maintaining Φ at 0.7 eV, similar to that of the pristine Alq₃.

Figure 3 shows the proposed energy band diagram for the pristine Alq₃ and 10% Rb₂CO₃-doped Alq₃ thin films obtained from the results in Fig. 2(b). Here, the ionization potential, the energy band gap (E_g), and the Φ_B^e , which is defined as the difference between the LUMO level and E_F of the electrode, of the pristine Alq₃ were taken as 5.7, 2.9, and 0.8 eV from the literature.⁶ Due to the reduction of Φ by the doping of Rb₂CO₃ in Alq₃ thin films as shown in Fig. 2(b), Φ_B^e could be reduced to 0.1 eV from 0.8 eV at these interfaces following the Rb₂CO₃ doping concentration of 10% and above in the Rb₂CO₃-doped Alq₃ thin films. Such low Φ_B^e is originated from the reduction of Φ , which is caused by the n -doping due to the interface dipole effect.⁶

To apply the results obtained in Figs. 1 and 2 to OLED devices, MoO_x-doped NPB was used as the hole-ohmic contact and the Rb₂CO₃-doped Alq₃ as the electron-ohmic contact. Figure 4 shows the J-V-L characteristics of the OLEDs with all carrier-ohmic contacts measured as a function of Rb₂CO₃ doping concentration in the Rb₂CO₃-doped Alq₃ thin film. The device structure was glass/ITO/MoO_x-doped NPB (25%, 5 nm)/NPB (63 nm)/Alq₃ (32 nm)/Rb₂CO₃-doped Alq₃ (x%, 10 nm)/Al (100 nm). The doping concentrations of Rb₂CO₃ in devices I, II, III, and IV were 0, 2.5, 10, and 50%, respectively. The J-V-L characteristics for devices I, II, III, and IV are also summarized in Table I. As shown in the table and Fig. 4, device III with the doping concentration of 10% exhibited the lowest turn-on voltage of 2.6 V at the luminance of 0.1 cd/m² among the devices investigated. In contrast, the devices with doping concentrations of either less than or greater than 10% showed higher turn-on voltages (V_T) than device III. Also, the maximum luminance (L_{max}) of devices I, II, III, and IV were 18 180 (at 11.6 V), 87 800 (at 10.8 V), 114 000 (at 9.8 V), and 39 140 (at 10.4 V), respectively. Figure 4(b) and Table I show power efficiency

TABLE I. Current density–voltage–luminance characteristics of the OLED devices according to the doping concentration of Rb₂CO₃ (%) in the Rb₂CO₃-doped Alq₃ thin film. The device structure was glass/ITO/MoO_x-doped NPB (25%, 5 nm)/NPB (63 nm)/Alq₃ (32 nm)/Rb₂CO₃-doped Alq₃ (x%, 10 nm)/Al (100 nm). The doping concentrations of the Rb₂CO₃ in devices I, II, III, and IV were 0, 2.5, 10, and 50%, respectively.

Device	Doping concentration of Rb ₂ CO ₃ (%)	V_T at 0.1 cd/m ²	η_{PE} (lm/W) at 1000 cd/m ²	L_{max} (cd/m ²)
I	0	3.0 V	0.8 at 8.4 V (36.4 mA/cm ²)	18 180 at 11.6 V
II	2.5	2.8 V	2.1 at 6.2 V (22.5 mA/cm ²)	87 800 at 10.8 V
III	10	2.6 V	2.7 at 5.4 V (21.3 mA/cm ²)	114 400 at 9.8 V
IV	50	2.6 V	2.0 at 5.6 V (24.3 mA/cm ²)	39 140 at 10.4 V

(η_{PE}) measured as a function of current density. The power efficiencies of devices I, II, III, and IV were 0.8, 2.1, 2.7, and 2.0 lm/W, respectively. The η_{PE} value increased from 0.8 to 2.7 lm/W as the doping concentration was increased from 0 to 10%, due to the increased n -doping effect in the Rb₂CO₃-doped Alq₃ thin films in addition to the reduction of Φ_B^e with increasing doping concentration of Rb₂CO₃. However, as the doping concentration was further increased from 10 to 50%, the η_{PE} decreased from 2.7 to 2.0 lm/W and the J-V-L characteristics degraded. When the doping concentration of Rb₂CO₃ was increased higher than 10%, Φ_B^e remained at 0.1 eV, but due to the significant chemical reaction, the interface properties degraded, resulting in the poor device performances of the OLED devices for doping concentrations greater than 10%. In Fig. 1, the J-V characteristics of the electron-only devices were degraded when the doping concentration of Rb₂CO₃ was increased beyond 10%. Therefore, light-emitting properties of V_T and η_{PE} shown in Fig. 4 and Table I are in good agreement with the results of

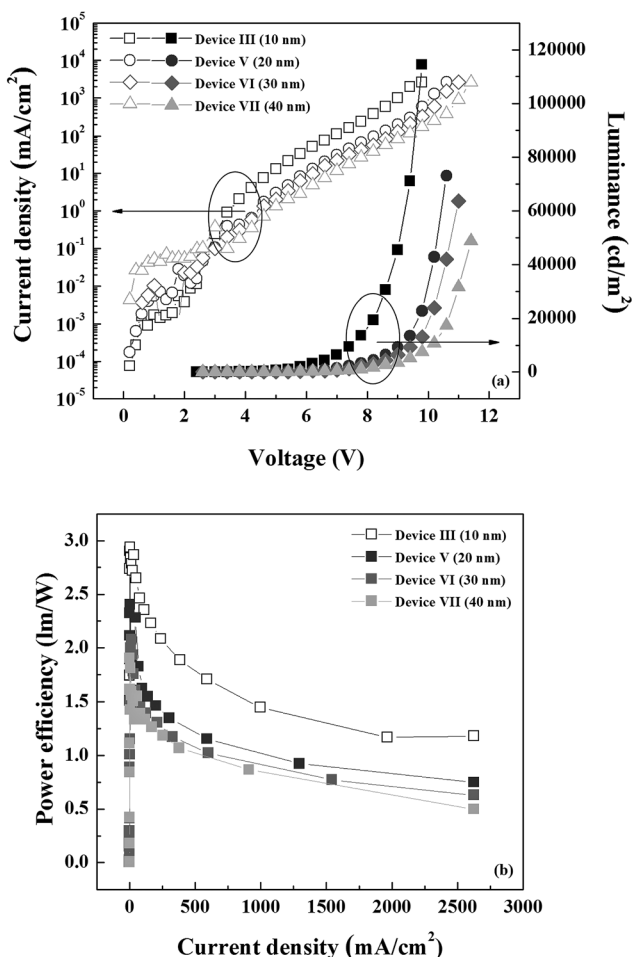


Fig. 5. (a) Current density–voltage–luminance characteristics in OLEDs with all carrier-ohmic contacts measured as a function of the thickness of the Rb₂CO₃-doped Alq₃ thin film at the doping concentration of 10%. The device structure was glass/ITO/MoO_x-doped NPB (25%, 5 nm)/NPB (63 nm)/Alq₃ (42-x nm)/Rb₂CO₃-doped Alq₃ (10%, y nm)/Al (100 nm). The thicknesses of the Rb₂CO₃-doped Alq₃ thin films in devices III, V, VI, and VII were 10, 20, 30, and 40 nm, respectively. (b) Power efficiency as a function of a current density.

TABLE II. Current density–voltage–luminance characteristics of the OLED devices according to the thicknesses of the Rb₂CO₃-doped Alq₃ thin films in the devices. The device structure was glass/ITO/MoO_x-doped NPB (25%, 5 nm)/NPB (63 nm)/Alq₃ (42-x nm)/Rb₂CO₃-doped Alq₃ (10%, x nm)/Al (100 nm). The thicknesses of the Rb₂CO₃-doped Alq₃ thin films in devices III, V, VI, and VII were 10, 20, 30, and 40 nm, respectively.

Device	Alq ₃ (42-x nm)/Rb ₂ CO ₃ -doped Alq ₃ (10%, x nm)	V _T at 0.1 cd/m ²	η_{PE} (lm/W) at 1000 cd/m ²	L _{max} (cd/m ²)
III	32/10 nm	2.6 V	2.7 at 5.4 V (21.3 mA/cm ²)	114 400 at 9.8 V
V	22/20 nm	3.0 V	1.8 at 6.8 V (25.0 mA/cm ²)	73 140 at 10.6 V
VI	12/30 nm	3.0 V	1.9 at 7.2 V (27.3 mA/cm ²)	63 660 at 11.0 V
VII	2/40 nm	3.2 V	1.5 at 7.8 V (26.5 mA/cm ²)	48 710 at 11.4 V

the electrical conductivity and interface mechanism, shown in Fig. 1.

Figure 5(a) shows the J-V-L characteristics in OLEDs with all carrier-ohmic contacts measured as a function of the thickness of the Rb₂CO₃-doped Alq₃ thin film at the doping concentration of 10%. The device structure was glass/ITO/MoO_x-doped NPB (25%, 5 nm)/NPB (63 nm)/Alq₃ (42-x nm)/Rb₂CO₃-doped Alq₃ (10%, y nm)/Al (100 nm). The thicknesses of the Rb₂CO₃-doped Alq₃ thin films in devices III, V, VI, and VII were 10, 20, 30, and 40 nm, respectively. As shown in Fig. 5(a), device III showed the highest current density. Also, the V_T of devices III, V, VI, and VII were 2.6, 3.0, 3.0, and 3.2 V, respectively; therefore, device III showed the lowest V_T. These results mean that the Rb₂CO₃-doped Alq₃ thin film functions as a resistor; thus, a higher electrical performance is obtained with a low-thickness Rb₂CO₃-doped Alq₃ thin film. The J-V-L characteristics of devices III, V, VI, and VII are also summarized in Table II. The L_{max} values of devices III, V, VI, and VII were 114 400 (at 9.8 V), 73 140 (at 10.6 V), 63 660 (at 11.0 V), and 48 710 (at 11.4 V) cd/m², respectively. Therefore, when the thickness was changed from 10 to 40 nm, considering both the V_T and L_{max}, device III with the 10 nm-thick Rb₂CO₃-doped Alq₃ thin film exhibited the highest device performance. Figure 5(b) and Table II show the η_{PE} measured as a function of current density. Device III in the η_{PE} also showed the highest efficiency of 2.7 lm/W among the devices investigated. The increased thickness of the Rb₂CO₃-doped Alq₃ (10%) film at constant total thickness of EIL/ETL [Rb₂CO₃-doped Alq₃ (10%) + Alq₃] decreases the total resistance of the device; therefore, the improvement of the device characteristics might be expected. However, as shown in Fig. 5, the lower performance of the device was observed in our experiment with the increase of thickness of the Rb₂CO₃-doped Alq₃ thin film at the same thickness of the EIL/ETL. The lower device performance might be related to the decrease of EML thickness responsible for the recombination of the carriers even though the increased thickness of the Rb₂CO₃-doped Alq₃ layer at constant total EIL/ETL thickness enhanced the electron injection and transport in the OLED. However, the exact reason may need to be investigated further. If the performances of our devices are compared with the devices investigated by other researchers, even though the devices in this study did not show performances as good as those of the Bphen-based devices reported by other researchers,¹⁹ they were better than those of the devices with LiF/Al cathode structures, which are most commonly studied.^{25,29,30}

IV. CONCLUSIONS

The Rb₂CO₃-doped Alq₃ thin film was investigated as a potential electron-ohmic contact material in OLEDs. UPS analyses revealed that the Φ_B^e , which occurs between electrodes and the Rb₂CO₃-doped Alq₃ thin film, was dramatically reduced as the Rb₂CO₃ doping concentration in the Rb₂CO₃-doped Alq₃ thin film was increased to 10% due to the reduction of the Φ by the n-doping effect. However, the increase of Rb₂CO₃ doping concentration from 10 to 50% did not change Φ_B^e , although it increased the decomposition of Alq₃ molecules; therefore, the interface characteristics were degraded, and the J-V characteristics of electron-only devices and the J-V-L characteristics of OLED devices with the Rb₂CO₃-doped Alq₃ thin films as the electron-injecting layer were degraded by increasing the doping concentration beyond 10%. The OLED consisting of glass/ITO/MoO_x-doped NPB (25%, 5 nm)/NPB (63 nm)/Alq₃ (32 nm)/Rb₂CO₃-doped Alq₃ (10%, 10 nm)/Al (100 nm) structure showed the highest light out-coupling characteristic with the L_{max} of 114 400 cd/m² at 9.8 V and η_{PE} of 2.7 lm/W at 1000 cd/m², among the other devices mentioned.

ACKNOWLEDGMENTS

This work was supported in part by the World Class University program of National Research Foundation of Korea (Grant No. R32-10124) and the Industrial Strategic technology development program (10041926, Development of high density plasma technologies for thin film deposition of nanoscale semiconductor and flexible display processing) funded by the Ministry of Knowledge Economy (MKE, Korea).

- ¹C. W. Tang and S. A. VanSlyke, *Appl. Phys. Lett.* **51**, 913 (1987).
- ²C. W. Tang, *Appl. Phys. Lett.* **48**, 183 (1986).
- ³F. Ebisawa, T. Kurokawa, and S. Nara, *J. Appl. Phys.* **54**, 3255 (1983).
- ⁴L. Wang, D. Fine, D. Sharma, L. Torsi, and A. Dodabalapur, *Anal. Bioanal. Chem.* **384**, 310 (2005).
- ⁵S. R. Forrest, *Nature* **428**, 911 (2004).
- ⁶H. Ishii, K. Sugiyama, E. Ito, and K. Seki, *Adv. Mater.* **11**, 605 (1999).
- ⁷L. C. Palilis, M. Uchida, and Z. H. Kafafi, *IEEE J. Sel. Top. Quantum Electron.* **10**, 79 (2004).
- ⁸M. Pfeiffer, S. R. Forrest, K. Leo, and M. E. Thompson, *Adv. Mater.* **14**, 1633 (2002).
- ⁹X. Zhou, J. Blochwitz, M. Pfeiffer, A. Nollau, T. Fritz, and K. Leo, *Adv. Funct. Mater.* **11**, 310 (2001).
- ¹⁰W. Gao and A. Kahn, *Appl. Phys. Lett.* **79**, 4040 (2001).
- ¹¹J. Huang, M. Pfeiffer, A. Werner, J. Blochwitz, K. Leo, and S. Liu, *Appl. Phys. Lett.* **80**, 139 (2002).
- ¹²M. Pfeiffer, K. Leo, X. Zhou, J. S. Huang, M. Hofmann, A. Werner, and J. B. Nimoth, *Org. Electron.* **4**, 89 (2003).

- ¹³K. Walzer, B. Maennig, M. Pfeiffer, and K. Leo, *Chem. Rev.* **107**, 1233 (2007).
- ¹⁴T. Matsushima and C. Adachi, *J. Appl. Phys.* **103**, 34501 (2008).
- ¹⁵D.-S. Leem, H.-D. Park, J.-W. Kang, J.-H. Lee, J. W. Kim, and J.-J. Kim, *Appl. Phys. Lett.* **91**, 011113 (2007).
- ¹⁶X. L. Zhu, J. X. Sun, H. J. Peng, Z. G. Meng, M. Wong, and H. S. Kwok, *Appl. Phys. Lett.* **87**, 153508 (2005).
- ¹⁷C.-C. Chang, M.-T. Hsieh, J.-F. Chen, S.-W. Hwang, and C. H. Chen, *Appl. Phys. Lett.* **89**, 253504 (2006).
- ¹⁸W.-J. Shin, J.-Y. Lee, J. C. Kim, T.-H. Yoon, T.-S. Kim, and O.-K. Song, *Org. Electron.* **9**, 333 (2008).
- ¹⁹M.-H. Chen, Y.-H. Chen, C.-T. Lin, G.-R. Lee, C.-I. Wu, S.-S. Leem, J.-J. Kim, and T.-W. Pi, *J. Appl. Phys.* **105**, 113714 (2009).
- ²⁰C.-I. Wu, C.-T. Lin, Y.-H. Chen, M.-H. Chen, Y.-J. Lu, and C.-C. Wu, *Appl. Phys. Lett.* **88**, 152104 (2006).
- ²¹P.-C. Kao, J.-H. Lin, J.-Y. Wang, C.-H. Yang, and S.-H. Chen, *J. Appl. Phys.* **109**, 094505 (2011).
- ²²M. Pfeiffer, A. Beyer, and K. Leo, *Appl. Phys. Lett.* **73**, 3202 (1998).
- ²³J. W. Kwon, J. T. Lim, and G. Y. Yeom, *Thin Solid Films*, **518**, 6339 (2010).
- ²⁴X. D. Feng, C. J. Huang, V. Lui, R. S. Khangura, and Z. H. Lu, *Appl. Phys. Lett.* **86**, 143511 (2005).
- ²⁵G. Parthasarathy, C. Shen, A. Khan, and S. R. Forrest, *J. Appl. Phys.* **89**, 4986 (2001).
- ²⁶F.-C. Chiu, H.-W. Chou, and J. Y.-M. Lee, *J. Appl. Phys.* **97**, 103503 (2005).
- ²⁷C. Shen, A. Khan, and J. Schwartz, *J. Appl. Phys.* **89**, 449 (2001).
- ²⁸M. G. Mason, C. W. Tang, L.-S. Hung, P. Raychaudhuri, J. Madathil, and D. J. Giesen, *J. Appl. Phys.* **89**, 2756 (2001).
- ²⁹Y. Q. Zhao, C. J. Huang, T. Ogundimu, and Z. H. Lu, *Appl. Phys. Lett.* **91**, 103109 (2007).
- ³⁰M. G. Helander, Z. B. Wang, and Z. H. Lu, *Appl. Phys. Lett.* **93**, 83311 (2008).